Research Square

Preprints are preliminary reports that have not undergone peer review.
They should not be considered conclusive, used to inform clinical practice,
or referenced by the media as validated information.

Is the QED Running a Slice of Geometric Modes? A Zero-Fit Fingerprint Test

shiwei xu

921902102@qq.com

1. Independent Researcher https://orcid.org/0009-0003-4910-0002

Research Article

Keywords: fine-structure constant; QED running; Bessel zeros; sonar fingerprint; zero-fit inversion; shape isomorphism

Posted Date: November 6th, 2026

DOI: https://doi.org/10.21203/rs.3.rs-11634902/v1

License: This work is licensed under a Creative Commons Attribution 4.0 International License.
Read Full License

Additional Declarations: The authors declare potential competing interests as follows: Conflict of Interest / Competing Interests The author of this paper is also the proposer of the proposition under test, namely the claim that the QED α running is the N = 1 slice of the ExB-T modal spectrum, as stated in Chapter 32, §32.6 of the original work [1], and the author is the author of the ExB-T theory series [1–13] from which that proposition originates. This dual role constitutes a potential conflict of interest, in that the verification process may be exposed to implicit confirmation bias. To mitigate this, the following measures were adopted: (1) all data, code, and figures are made publicly available so that any third party can independently reproduce the results; (2) the final definitions and thresholds of the fingerprint criteria were fixed before the results were computed; (3) the boundary statements in §4.4 explicitly distinguish shape isomorphism (weak sense) from mechanistic identity, so that the conclusions are not overstated; and (4) the limitations of the verification, including the author's dual role, are disclosed in §4.5. The author does not claim third-party independence. The validity of the verification rests on the reproducibility of the computational process, not on the identity of the verifier. Independent third-party verification is invited and would further reduce the risk of confirmation bias, but is not treated as a necessary condition for theoretical verification.

Is the QED Running a Slice of Geometric Modes? A Zero-Fit Fingerprint Test

Xu Shiwei

November 2026

Abstract This paper uses a zero-fit inversion to test the proposition that the α running curve computed from the geometric modes of the original paper [1] is isomorphic to the QED 1–5 loop α running curve. The α sequence computed in [1] in order of the mode index L (L = 1–330) is inverted to the energy scale μ using standard β-function coefficients from the literature (consistent with the experimental running); this paper examines the segment-by-segment shape isomorphism between $\ln(\mu)$ and the geometric-side $\ln(u)$, where u is the first nonzero root of j_L (ground state, L = 1–330). Since the inversion is reversible, this test is equivalent to an indirect verification of the original proposition. The segmental residuals of the last 5 segments are $\leq 2\%$, and the variation of each metric across 1–5 loops is $< 1.5\%$. Five classes of fingerprint metrics (DTW, derivative, inflection point, curvature, segmental residual) and three steepness metrics (front-segment slope ratio, sagitta-to-chord ratio relative difference, crossing point) all indicate that the two sequences are isomorphic in shape, with the 5-loop case serving as supplementary verification. The results support, at the methodological level defined in §1.3, the shape-level validity of the original proposition; this paper does not claim mechanistic identity (shape isomorphism is used in a weak sense; see §1.1). The author is also the proposer of that proposition and does not claim third-party independence; the validity of the verification rests on the reproducibility of the computational process, not on the identity of the verifier.

ORCID: 0009-0003-4910-0002. Email: xushiweijiangxiaorong@gmail.com. Panzhihua, Sichuan Province, China.

Panzhihua, Sichuan Province, China

Keywords fine-structure constant; QED running; Bessel zeros; sonar fingerprint; zero-fit inversion; shape isomorphism

1 Introduction: The Question in the Title and a Testable Proposition

1.1 Origin of the Question in the Title

The question in the title concerns the proposition stated in Chapter 32, §32.6 of the original paper, *Shi Yuan Fan—The Universe Governed by* $\varphi\pi e$ [1]. The proposition is stated as follows:

"The α running of QED is exactly equal to the modal α sequence arranged in L order on the $N = 1$ shell. The QED running is the $N = 1$ slice of the ExB-T modal spectrum." [1]

This proposition originates from the ExB-T series of papers [1–13]. That series comprises works within the same theoretical framework; this paper does not review their contents one by one, but uses them only as the source of the proposition under test. The original wording is quoted only here, and the methods, parameters, or conclusions of the original paper are not assessed below; the verification method of this paper is independent of any forward computation in the original paper.

"Shape isomorphism" in this paper is used in a weak sense: it means that two normalized curves are indistinguishable in shape, not that a structure-preserving bijection exists in the strict mathematical sense. Throughout, "isomorphism" is used in this weak sense. Likewise, "mechanistic identity" means identity of physical mechanism.

1.2 Operationalization of the Proposition

The original proposition can be stated as: the α sequence obtained from the geometric modes of the $N = 1$ shell computed in the original paper yields a running curve equivalent to the QED 1–5 loop α running curve, i.e., the two are isomorphic in a weak sense. This paper operationalizes it into computable criteria:

1. Geometric side: this paper takes the first nonzero root u of the spherical Bessel function $j_L(x)$ ($n = 1$, i.e., the ground state) for $L = 1$–330, and constructs the sequence $\ln(u)$. This sequence is a purely geometric quantity containing no QED input.
2. QED side: this paper takes the α sequence from Table 02 of the original paper [1] ($L = 1$–330, computed in the original paper via a nonlinear formula and Bessel geometric modes, not experimentally measured values), and inverts it to the energy scale μ via analytic integration with the standard QED β-function coefficients from the literature, constructing the sequence $\ln(\mu)$. The β coefficients are standard values consistent with the experimental running and are not derived from the original paper.
3. Comparison: each sequence is min–max normalized to $[0, 1]$, and segment-by-segment shape isomorphism is tested under sonar fingerprint criteria.

If the original proposition holds, the two normalized curves should exhibit comparable shape structure. This paper tests this shape isomorphism and does not test mechanistic identity.

Since the inversion is reversible, testing the isomorphism between $\ln(\mu)$ and $\ln(u)$ is equivalent to an indirect test of the proposition that the α running curve of the original paper is isomorphic to the QED 1–5 loop α running curve (see §1.3 for an explanation of the reverse-verification strategy).

1.3 Positioning of This Paper, Reverse-Verification Strategy, and Disclosure of Author Identity

This paper is a theoretical verification, not a mechanistic proof. The validity of the verification rests on the reproducibility of the computational process: all data, code, and figures are provided with the paper, and any reader can independently re-run all results. This paper does not claim third-party independence; the author's identity does not affect the reproducibility of the computational process.

This paper adopts a reverse-verification strategy: rather than directly comparing the α sequence of the original paper with the geometric modes (to avoid the "fitting" objection), it uses standard β coefficients from the literature to invert α to the energy scale μ and tests the isomorphism between $\ln(\mu)$ and $\ln(u)$. The β coefficients are consistent with the experimental running, and the inversion is reversible, so this test is equivalent to an indirect verification of the original proposition: if $\ln(\mu)$ and $\ln(u)$ are isomorphic, then the proposition that the α running curve of the original paper is isomorphic to the QED 1–5 loop α running curve holds.

Methodologically, the failure of a theoretical verification does not constitute a logical refutation (theoretical holism in the Lakatosian framework [25]), and replication is less essential in theoretical work than in experimental work; the reward structure of science makes reproducibility problems inevitable [24], so reproducibility is a reasonable basis for theoretical verification. "At the methodological level" in this paper means that the support for the proposition rests on the reproducibility of the computation, not on independent authorship.

It must be explicitly disclosed that the author of this paper is also the proposer of the proposition under test. This dual role means that the verification process is exposed to potential confirmation bias; this is discussed in §4.5, together with the mitigation measures adopted to reduce it.

1.4 Contributions of This Paper

1. Reverse-verification strategy: using standard β coefficients from the literature to invert the α sequence of the original paper to the energy scale and testing the isomorphism between $\ln(\mu)$ and $\ln(u)$, avoiding the fitting objection that arises from directly comparing α sequences.
2. Fingerprint criteria: replacing global correlation metrics with five classes of fingerprint metrics and three steepness metrics to test segment-by-segment shape isomorphism rather than monotonicity correlation.
3. Order stability (stability with respect to loop order) across 1–5 loops: 1–4 loops are the main results, and the 5-loop case is supplementary verification (β_4 taken from Kataev and Larin 2012 [17]), demonstrating that the fingerprint metrics do not collapse under higher-order corrections.
4. One-click reproducibility package: data, code, and figures are all provided in *ExB-T Zero-Fit Verification_One-Click Reproduction.xlsx*.

2 Methods: Zero-Fit Inversion and Fingerprint Criteria

2.1 Geometric Side: Ground-State Zero Sequence of Spherical Bessel Functions

On the geometric side, this paper takes the first nonzero root $u_{L,1}$ of the spherical Bessel function $j_L(x)$ for $L = 1$–330, with $N = 1$ (ground state). Each L corresponds to one ground-state zero; the sequence $\ln(u)$ is the logarithmic sequence of these 330 ground-state zeros. This sequence is a deterministic geometric quantity containing no QED parameters, experimental data, or fitting degrees of freedom. The 330 modes for $L = 1$–330 are in one-to-one correspondence with the α sequence on the QED side.

Rigorous enclosure results exist for the asymptotic behavior of Bessel functions and their derivative zeros [27]; this paper takes the first nonzero root over the range $L = 1$–330 and does not rely on the specific form of the asymptotic expansion.

2.2 QED Side: Analytic Inversion of the α Sequence of the Original Paper

For the running of the fine-structure constant α and its history, see [29]; the QED-side α sequence in this paper is taken from Table 02 of [1], consisting of modal α values computed in the original paper in L order, not experimentally measured values. This paper takes this α sequence as input and inverts it to the energy scale μ via analytic integration with standard β coefficients from the literature. The β coefficients are standard values consistent with the experimental running [14–18] and are not derived from the original paper; the inversion process is zero-fit (no free parameters), but the upstream α values are computed in the original paper. The β-function expansion is:

$$\frac{dt}{d\ln\mu} = \beta_0 t^2 + \beta_1 t^3 + \beta_2 t^4 + \beta_3 t^5 + \beta_4 t^6, \qquad t = \alpha/\pi \tag{1}$$

The inversion formula is:

$$\ln(\mu/\mu_0) = \int_{\alpha_0/\pi}^{\alpha/\pi} \frac{dt}{\beta(t)} \tag{2}$$

The β coefficients are standard literature values, listed below:

Convention: in this paper $\beta_i = c_i/2$, where c_i are the standard coefficients ($c_0 = 2/3$, so $\beta_0 = 1/3$ under this convention). The value of β_4 under this paper's convention is -0.54492; for the standard c_4 see [17]. The complete five-loop calculations of β_3 and β_4 are given in [18] (preprint), and the numerical values as used in [1] are cited here for reproducibility. Reference point: $\alpha_0 = \alpha(L = 1) = 0.007297352565157$, $\mu_0 = 1$. Numerical integration is performed with `scipy.integrate.quad` (`epsabs=1e-15`, `epsrel=1e-15`, `limit=500`).

Table 1 β coefficients and literature sources

Coefficient	Value	Literature source
β_0	$1/3$	[14]
β_1	$1/4$	[15]
β_2	$-31/288$	[16]
β_3	$-(2785/31104 + 13\zeta_3/36)$	[18]
β_4	-0.54492	[17,18]

The 1-loop analytic solution $\ln(\mu/\mu_0) = 3\pi(1/\alpha_0 - 1/\alpha)$ serves as a benchmark for the numerical integration; the maximum relative error in the 1-loop check is 4.24×10^{-15}, and the inversion residual is 0.

The β coefficients are literature values, and the inversion is analytic and reversible. This paper performs no fitting of the β coefficients and does not align or adjust the α sequence.

Since the inversion is reversible, testing the isomorphism between $\ln(\mu)$ and $\ln(u)$ is equivalent to an indirect test of the proposition that the α running curve of the original paper is isomorphic to the QED 1–5 loop α running curve.

2.3 Normalization

Each sequence is min–max normalized to $[0, 1]$. This step corresponds to the amplitude/channel normalization used as preprocessing in acoustic fingerprint recognition: removing the overall scale freedom so that subsequent comparison addresses shape structure rather than absolute amplitude. Normalization is a preprocessing step for fingerprint comparison and does not constitute an additional assumption about similarity; similarity is measured by the fingerprint metrics after normalization, not produced by normalization itself.

2.4 Fingerprint Criteria

The comparison of curves as data objects is well established in functional data analysis and shape analysis [22,30]; recent reviews of curve similarity methods also exist [31]. Within this framework, this paper selects

DTW, derivatives, curvature, and segmental residuals as fingerprint criteria.

2.4.1 Five Classes of Fingerprint Metrics

Table 2 Five classes of fingerprint metrics

Category	Metric	Description
1. DTW alignment	DTW distance, residual max/mean, path offset	Dynamic time warping [21], Sakoe–Chiba band = 30
2. Derivative correlation	Pearson, Spearman, residual	Forward difference d/dL
3. Inflection point comparison	Count, L coordinate, alignment error	Sign changes of the second difference
4. Curvature comparison	Corr, residual max	$\kappa = \lvert y'' \rvert / (1 + y'^2)^{3/2}$; recent results on the asymptotics of derivative zeros see [28]
5. Segmental residual	6 segments, mean/RMS/Corr	Approximately 55 points per segment

2.4.2 Three Steepness Metrics

Table 3 Three steepness metrics

Metric	Definition
Front-segment slope ratio	Ratio of the mean slope of u to that of μ over $L = 1$–55
Sagitta-to-chord ratio relative difference	Relative difference in curve bending degree (%); see Fig. 6
Crossing point	Position (by linear interpolation) of the zero crossing of the difference between the two curves

2.4.3 Methodological Sources and Justification of Applicability

The five classes of fingerprint metrics above (DTW, derivative, curvature, segmental residual) are mature acoustic fingerprint tools for underwater target recognition [19,20]. Sonar fingerprint comparison usually presupposes that the two sequences originate from the same physical source and are transmitted through different channels. This paper does not rely on the premise of "the same physical source," but instead uses the fingerprint criteria only for their sensitivity to shape structure, to test whether the two sequences exhibit a detectable shape consistency. This consistency is a prediction implied by the criteria, not a premise of their validity—if the original proposition holds, the consistency should be detected; if it does not hold, it should not be detected. Used in this way, the fingerprint criteria test shape isomorphism and do not presuppose mechanistic identity. This paper is not aware of prior use of this combination of tools for comparing sequences of geometric zeros with QED energy-scale sequences.

2.5 Classification of Metrics into Three Groups

To avoid the objections of "metric stacking" and "post hoc metric selection," all metrics are classified into three groups in this paper:

1. Primary metrics: five classes of fingerprint metrics and three steepness metrics. The main conclusions rely only on this set.
2. Auxiliary metrics: logarithmic-family b ratio (depends on the choice of fitting function, used as an auxiliary reference only; not used in the main results).
3. Descriptive metrics: saturation point position difference (low information content), global R^2/Corr/CosSim (insensitive to local structure).

Both table notes and the main text state that auxiliary and descriptive metrics are not used as standalone criteria.

2.6 Reproducibility

All data, code, and figures are provided in *ExBT Zero-Fit Verification_One-Click Reproduction.xlsx*, containing worksheets 00–10 (cover, methods, global metrics, sonar fingerprint, steepness metrics, point-by-point verification, five-loop comparison, segmental residuals, figures, reproduction code, raw data). Any reader can re-run all computations.

3 Results

3.1 Global Metrics (Auxiliary Reference)

Table 4 presents the global metrics, which are almost unchanged from 1 to 5 loops:

Global metrics are an auxiliary reference, and the main conclusions do not depend on this set. Note: global metrics are insensitive to local structure—two

Table 4 Global metrics (1–5 loops)

Loops	R^2	RMSE	MAE	Corr	CosSim
1 loop	0.981719	0.029787	0.016139	0.998247	0.999356
2 loops	0.981850	0.029673	0.016081	0.998245	0.999360
3 loops	0.981850	0.029674	0.016081	0.998245	0.999360
4 loops	0.981850	0.029674	0.016081	0.998245	0.999360
5 loops	0.981850	0.029674	0.016081	0.998245	0.999360

monotonically increasing curves can still achieve a high R^2 even if their local shapes differ. Therefore, this paper does not use global metrics as the primary criterion for shape isomorphism.

3.2 Fingerprint Metrics (Primary)

DTW alignment: the DTW distance is 0.32424 for 1 loop and 0.32385 for 2–5 loops; the residual mean is 9.4×10^{-4}; the maximum path offset is 10, within band = 30. The path offset accounts for about 3% of the full range, reflecting a local alignment difference between the two curves in the low-L segment, consistent with the location of the absolute-difference peak in §3.4.

Derivative correlation: the Pearson correlation is 0.93611 for 1 loop and 0.93615 for 2–5 loops; the Spearman rank correlation is identical for all five loops (0.9999946). The gap between Pearson and Spearman is itself informative: the ranks are almost completely consistent while the amplitudes differ, indicating that the two derivative sequences are "same order, different local slopes." This is precisely the right description of "shape-isomorphic, numerically unequal," and provides more structural information than a single global correlation.

Inflection point comparison: the number of inflection points is an integer and is sensitive to small curvature fluctuations. The geometric-side $\ln(u)$ increases monotonically with a slope that decreases as L increases (the second difference is negative), with no sign change throughout, yielding zero inflection points; the QED-side $\ln(\mu)$ exhibits slight fluctuations at the low-L end due to truncation of the β coefficients, yielding two inflection points ($L = 5, 7$), consistent across 1–5 loops. This difference arises from residual higher-order corrections on the QED side and does not contradict shape isomorphism—in the later segment ($L > 10$) neither curve has inflection points, and the shapes agree.

Curvature comparison: curvature Corr 0.82504, residual max 0.00844. The curvature correlation is lower than that of first-order quantities (derivative, DTW), an expected decrease for a second-order quantity (which is more sensitive to noise), and still constitutes a strong correlation.

Segmental residuals: the minimum segmental Corr is 0.99009, stable across five loops; segments 2–6 have Corr $\geq$ 0.99994.

3.3 Steepness Metrics (Primary)

Table 5 Steepness metrics (1 loop and 2–5 loops)

Metric	1 loop	2–5 loops
Front-segment slope ratio (u/μ)	1.0679	1.0673
Sagitta-to-chord ratio relative difference (%)	5.146	5.077
Crossing point L	151.02	149.43

A front-segment slope ratio > 1 indicates that the geometric-side curve is steeper in the front segment; a sagitta-to-chord ratio relative difference of about 5% indicates that the bending degrees of the two curves differ by about 5%; the crossing point is $L = 151.02$ for 1 loop and $L = 149.43$ for 2–5 loops. Together, the three metrics characterize the shape feature of "a slight difference in front-segment steepness and agreement in the later segment."

3.4 Point-by-Point Verification

The point-by-point absolute difference peaks at 0.0958 at $L = 12$, corresponding to 9.6% of the normalized amplitude; the two curves cross at $L = 151$ (difference 2.86×10^{-6}, i.e., to numerical precision); the peak residual in the later segment is 0.42% at $L = 224$. At the very low L end ($L < 10$), the relative difference is amplified because the denominator is small, and interpretation is based on the absolute difference.

The distribution of point-by-point differences shows a single-peaked profile of "large in the front segment, small in the later segment": the absolute difference over L = 2–55 rises from 0.0076 to 0.0958 and then falls to 0.0387; after crossing zero at $L = 151$ the sign reverses, and for $L > 160$ the absolute difference is $\leq$ 0.0038. This distribution is consistent with the discussion in §4.1.

3.5 Segmental Residuals

Table 6 presents the 6-segment segmental residuals (1 loop):

The mean residual of segment 1 is 0.0656, and that of the last 5 segments is $\leq$ 0.0201; the Corr of

Table 6 Segmental residuals (1 loop, $L = 1$–330 divided into 6 segments)

Segment	L range	Mean residual	RMS residual	Segment Corr
1	1–55	0.0656	0.0693	0.99008
2	56–110	0.0204	0.0221	0.99994
3	111–165	0.0028	0.0037	0.99995
4	166–220	0.0031	0.0032	0.99997
5	221–275	0.0035	0.0035	0.99998
6	276–330	0.0015	0.0017	0.99998

each segment is ≥ 0.990, and that of segments 2–6 is ≥ 0.99994. Segment 1 is the only segment with a relatively high residual, corresponding to the steepness difference at the low-L end; §4.1 discusses its source.

3.6 Order Stability

The variation of each metric across 1–5 loops is $< 1.5\%$:

Table 7 Five-loop ranges

Metric	Five-loop range	Percentage of mean (%)
Front-segment slope ratio	0.000554	0.05
Sagitta ratio relative difference	0.0689 percentage points	1.35
Crossing point L	1.6030	1.07
DTW distance	0.000395	0.12

Note: for the sagitta ratio, the range is given in percentage points because the metric itself is a percentage.

The crossing point converges from 2 loops onward (spread of 0.006 L units for 2–5 loops). The 5-loop case is supplementary verification (β_4 taken from Kataev and Larin 2012 [17]); all fingerprint metrics differ from the 4-loop case at the 10^{-5}–10^{-6} level, and all 1–5 loops are consistent, with no collapse. This paper does not claim that any particular loop is optimal.

3.7 Graphical Results

Figures 1–6 are given in Appendix A (see also worksheet 08_Figures in the supplementary xlsx), corresponding to the normalized curves, DTW alignment path, derivatives, curvature, segmental residuals, and steepness comparison, respectively. The figures are placed in the appendix to keep the main text compact.

4 Discussion

4.1 Source of the Front-Segment Steepness Difference

The relatively high residual in segment 1 ($L = 1$–55) corresponds to the front-segment steepness difference (slope ratio 1.067) in §3.3. Its possible sources are as follows:

The geometric-side j_L ground-state zeros depart from the asymptotic envelope relatively rapidly at the low-L end; the specific low-L computational behavior of the α sequence in the original paper is not assessed here. This geometric-side deviation decays together with the front-segment slope difference as L increases and does not affect the conclusions for the later segments. Under the zero-fit inversion framework, this paper does not attribute this difference to a unique physical cause, but merely records it as a parameter-level difference in the front segment of the two curves.

This difference is confined to the front segment; the conclusion of strong overlap in the last 5 segments is unaffected.

4.2 Forward Shift of the Crossing Point

The crossing point shifts from $L \approx 151.02$ for 1 loop to $L \approx 149.42$ for 2 loops, and then stabilizes at $L \approx 149.43$ (spread of 0.006 L units for 2–5 loops). This forward shift may be related to truncation of the β-function series: the 1-loop case includes only β_1, whereas from 2 loops onward β_2–β_4 are included, causing a slight adjustment of the QED-side curve in the low-L segment and thus a shift in the crossing point. The crossing point stabilizes after 2 loops, supporting this explanation. This convergence behavior serves as auxiliary evidence of order stability.

4.3 Physical Explanation of the Small Differences Across 1–5 Loops

With $\alpha/\pi \approx 0.003$, the change in $\ln(\mu)$ due to higher-order corrections is of order 10^{-5}, too small to significantly change the curve shape. The variation of less than 1.5% in each metric across 1–5 loops reflects order stability—the fingerprint metrics do not collapse when higher-order corrections are added—rather than any one loop being superior. This consistency itself constitutes evidence of theoretical self-consistency.

4.4 Boundary Statements

1. Zero-fit inversion does not imply a zero-fit upstream α: α is the modal value computed in the original paper in L order, not an experimental value; the β coefficients are standard literature values consistent with the experimental running, not derived from the original paper. The inversion is an

analytically reversible transformation that neither adds nor removes any physical content. "Zero-fit" in this paper means that the inversion process has no free parameters, not that the upstream α values come from a zero-fit procedure or from experiment.
2. Shape isomorphism under fingerprint criteria does not imply mechanistic identity: this paper tests the segment-by-segment shape isomorphism (weak sense) of two normalized curves and does not claim a mathematical isomorphism or identity of physical mechanism between the energy scale and the Bessel zeros.
3. The 330 points are used as given in the data table: this paper does not address the physics of the 328/330 difference; all computations are based on the 330 points in the data table.
4. Fingerprint criteria are used for shape comparison only and do not constitute a proof of physical mechanism.

4.5 Limitations

1. Exploratory nature of the criteria: the final definitions and thresholds of the fingerprint criteria were determined before the results were obtained; the process of selecting the metrics was exploratory, and this paper discloses this.
2. Double-edged interpretation of order stability: the small differences across 1–5 loops, on the one hand, indicate that the fingerprint metrics do not collapse when higher-order corrections are added, constituting positive evidence of theoretical self-consistency; on the other hand, they also limit the resolution of "order stability" as a criterion—if higher-order corrections (e.g., the 6-loop β_5) were to introduce larger changes, they would provide a stronger constraint.
3. Figures placed in the appendix: the main text contains no figures; the graphical results are given in Appendix A.
4. Author identity overlap: the author of this paper is also the proposer of the proposition under test, and the verification process is exposed to potential confirmation bias. Self-generated hypotheses exhibit a systematic confirmation bias in testing [23]; publication pressure is also associated with reporting bias [26]. To mitigate this bias, this paper takes the following measures: (1) all data and code are made public so that any third party can independently reproduce them [24]; (2) the final definitions and thresholds of the fingerprint criteria were determined before the results were obtained; (3) the boundary statements in §4.4 clearly distinguish shape isomorphism from mechanistic identity. Independent third-party verification can further reduce confirmation bias but is not a necessary condition for theoretical verification [25].

5 Conclusion

5.1 Response to the Question in the Title

Under the fingerprint criteria, the answer is: yes—the α sequence computed from geometric modes in the original paper, when inverted, yields an energy scale that matches, segment by segment, the shape of the geometric-side $\ln(u)$ (the first nonzero root of j_L, ground state, $L = 1$–330). Under mechanistic criteria, this paper makes no assertion.

5.2 Support for the Original Proposition

The results of this paper support, at the methodological level defined in §1.3, the shape-level validity of the proposition stated in §1.1 (the author is also the proposer; see §1.3): the α sequence computed from geometric modes in the original paper, when inverted, yields an energy scale that matches, segment by segment, the shape of the geometric-side $\ln(u)$ (the first nonzero root of j_L, ground state); since the inversion is reversible, this result constitutes support for the proposition that the α running curve of the original paper is isomorphic to the QED 1–5 loop α running curve. It must be emphasized that "shape-level validity" means that the α running curve of the original paper and the QED running curve are indistinguishable in normalized shape; it does not mean that this paper proves the mechanistic claim that the energy scale equals the Bessel mode. This paper does not claim a mathematical isomorphism between the energy scale and the Bessel zeros, nor does it further discuss the mechanistic implications of such an isomorphism.

5.3 Outlook

Higher-loop corrections, other N values, other modal slices, and preregistration of the criteria are possible directions for future work.

Data availability

The data, code, and figures underlying this study are provided in *ExB-T Zero-Fit Verification_One-Click Reproduction.xlsx* (supplementary material) and will

be deposited in Zenodo upon acceptance; the DOI will be provided at proof stage.

A Graphical Results

Table 8 Figure files and their positions in the main text

Figure	File	Content	Position in main text
Figure 1	`fig1_curves.png`	$\ln(u)$_norm vs $\ln(\mu)$_norm (1–5 loops)	§3.1
Figure 2	`fig2_dtw.png`	DTW alignment path (1 loop, band = 30)	§3.2
Figure 3	`fig3_deriv.png`	Derivative sequence comparison (1 loop, forward difference d/dL)	§3.2
Figure 4	`fig4_curv.png`	Curvature sequence comparison (1 loop, $\kappa = \lvert y''\rvert/(1+y'^2)^{3/2}$)	§3.2
Figure 5	`fig5_segment.png`	6-segment segmental residuals (1 loop, $L = 1$–330 divided into 6 segments)	§3.2
Figure 6	`fig6_steep.png`	Steepness comparison (1–5 loops, annotated with $L = 12$, $L = 151$, $L = 224$, $L \approx 149.4$)	§3.3

Figure captions:

1. Figure 1: Comparison of normalized curves between the geometric-side $\ln(u)$_norm and the QED-side $\ln(\mu)$_norm (1–5 loops).
2. Figure 2: DTW alignment path (1 loop, band = 30).
3. Figure 3: Derivative sequence comparison (1 loop, forward difference d/dL).
4. Figure 4: Curvature sequence comparison (1 loop, $\kappa = \lvert y''\rvert/(1+y'^2)^{3/2}$).
5. Figure 5: 6-segment segmental residuals (1 loop, $L = 1$–330 divided into 6 segments).
6. Figure 6: Steepness comparison (1–5 loops, annotated with the $L = 12$ absolute-difference peak, the $L = 151$ crossing point, the $L = 224$ later-segment residual peak, and the $L \approx 149.4$ higher-order crossing point—i.e., the 2–5 loop crossing point).

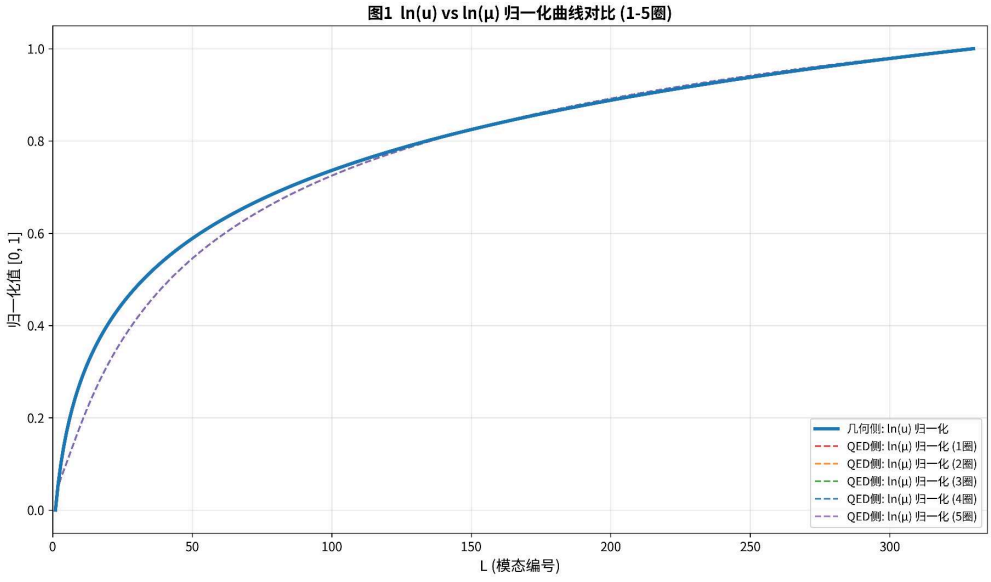


Fig. 1 Comparison of normalized curves between the geometric-side $\ln(u)$_norm and the QED-side $\ln(\mu)$_norm (1–5 loops).

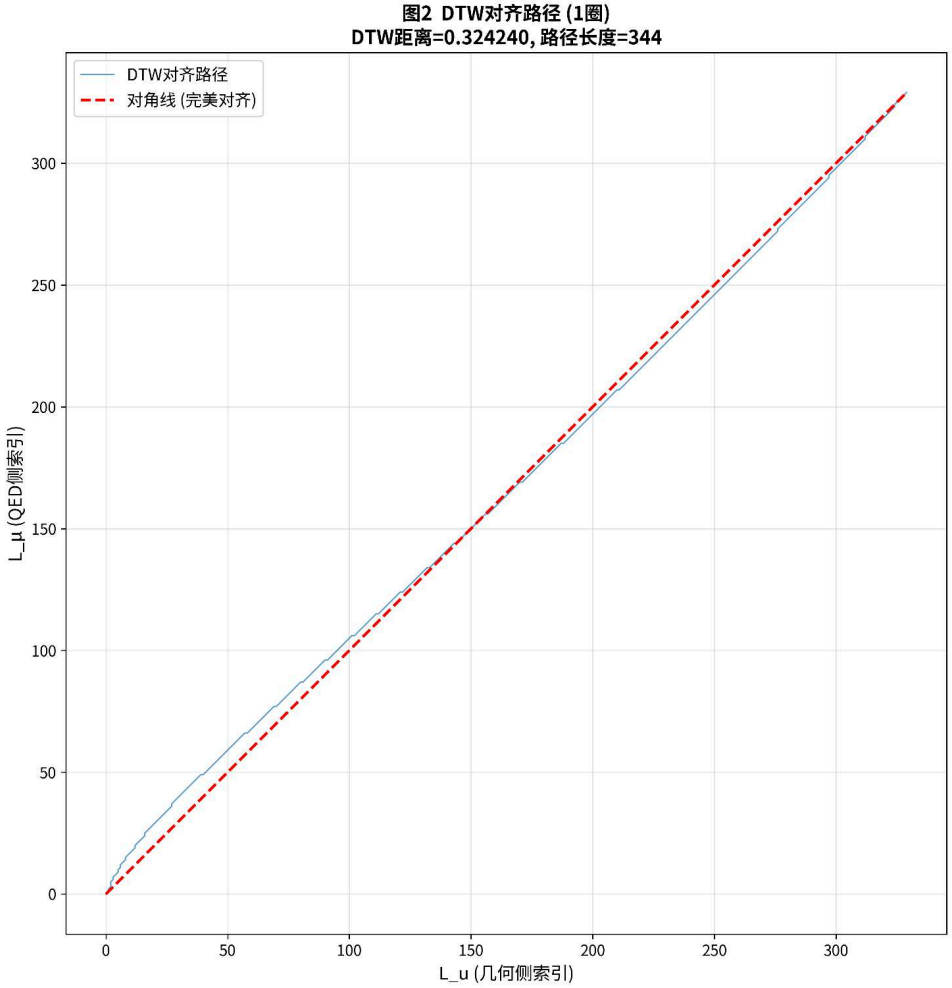


Fig. 2 DTW alignment path (1 loop, band = 30).

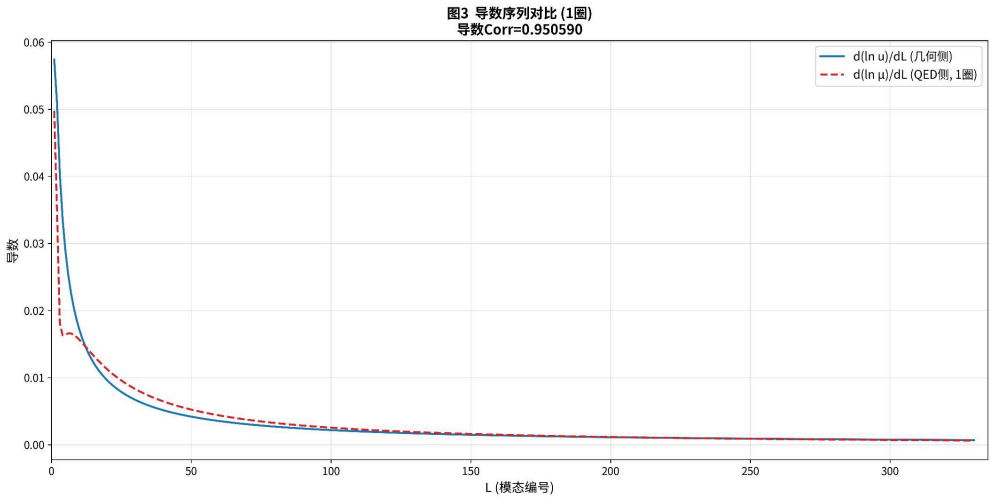


Fig. 3 Derivative sequence comparison (1 loop, forward difference d/dL).

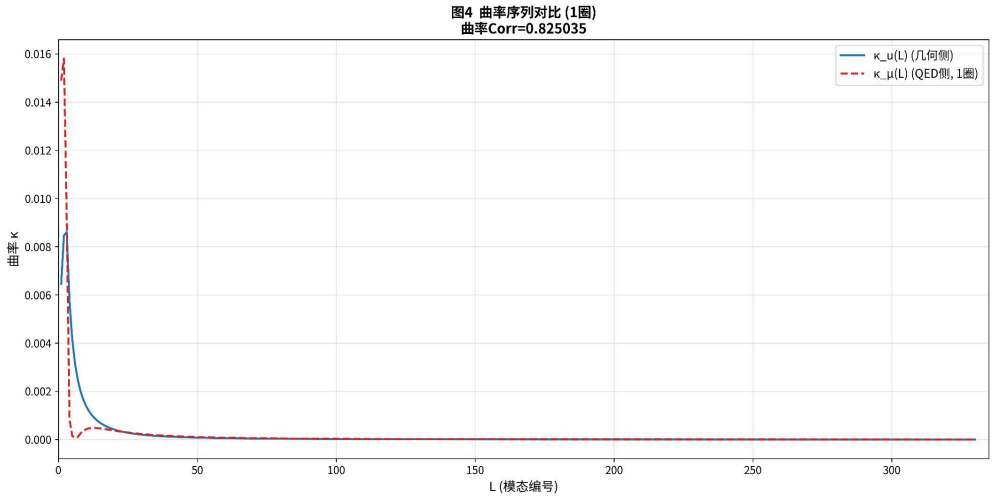


Fig. 4 Curvature sequence comparison (1 loop, $\kappa = |y''|/(1+y'^2)^{3/2}$).

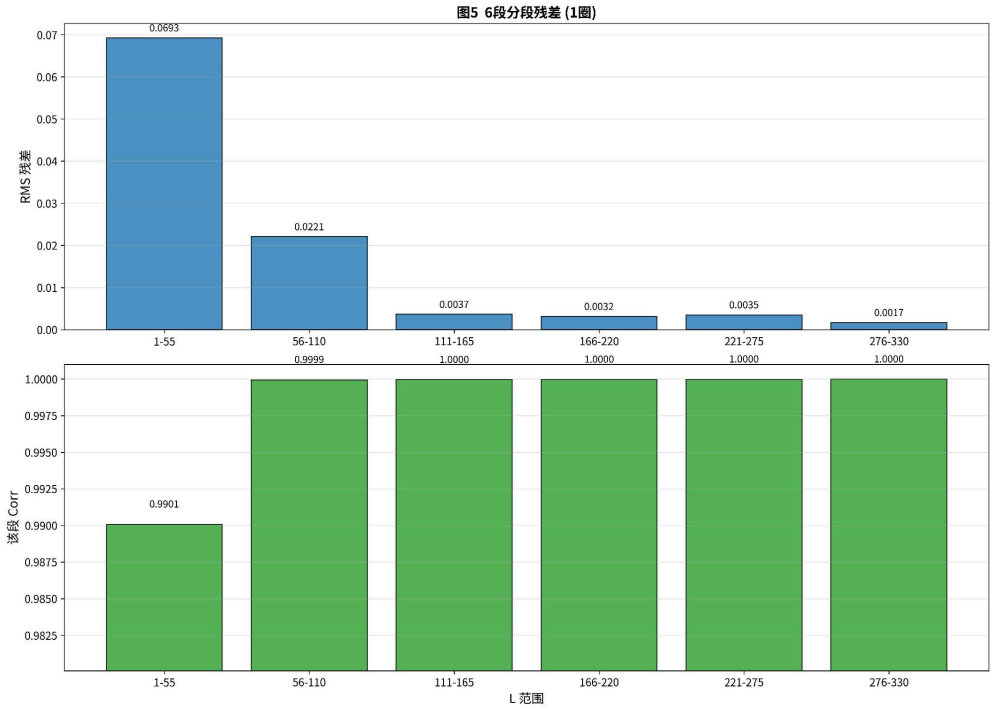


Fig. 5 6-segment segmental residuals (1 loop, $L = 1$–330 divided into 6 segments).

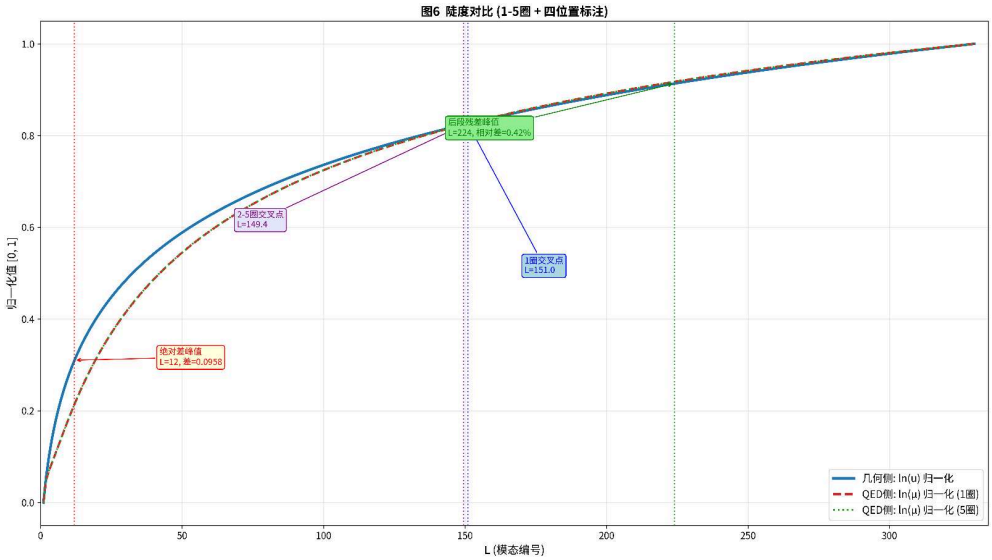


Fig. 6 Steepness comparison (1–5 loops, annotated with the $L = 12$ absolute-difference peak, the $L = 151$ crossing point, the $L = 224$ later-segment residual peak, and the $L \approx 149.4$ higher-order crossing point).

References

1. Xu S. Shi Yuan Fan—The Universe Governed by $\varphi\pi e$ (V3, 40-chapter monograph)[M/OL]. Zenodo, 2026. https://doi.org/10.5281/zenodo.20575318 [in Chinese]
2. Xu S. E×B-T spherical Bessel standing-wave solitons[M/OL]. Zenodo, 2026. https://doi.org/10.5281/zenodo.21695194 [in Chinese]
3. Xu S. E×B-T rotational-field solitons: the algebraic-geometric origin of spin-1/2 and the fine-structure constant[M/OL]. Zenodo, 2026. https://doi.org/10.5281/zenodo.21890626 [in Chinese]
4. Xu S. The geometric-topological origin of quantization—from standing waves to Möbius bands[M/OL]. Zenodo, 2026. https://doi.org/10.5281/zenodo.22688571 [in Chinese]
5. Xu S. Deriving quantum mechanics and the Dirac equation from ExB-T geometry—the quadruple structure of the circulation quantization condition[M/OL]. Zenodo, 2026. https://doi.org/10.5281/zenodo.22732331 [in Chinese]
6. Xu S. Three hundred years of the wave equation[M/OL]. Zenodo, 2026. https://doi.org/10.5281/zenodo.22769636 [in Chinese]
7. Xu S. Deriving special relativity from the ExB-T phase-locking condition[M/OL]. Zenodo, 2026. https://doi.org/10.5281/zenodo.22911927 [in Chinese]
8. Xu S. Deriving general relativity from ExB-T geometry—the unification of quantum theory and gravitational theory[M/OL]. Zenodo, 2026. https://doi.org/10.5281/zenodo.23072666 [in Chinese]
9. Xu S. The mathematical principles of motion—a mathematical proof of the first cause[M/OL]. Zenodo, 2026. https://doi.org/10.5281/zenodo.22900496 [in Chinese]
10. Xu S. Deriving general relativity from wave ontology—intrinsic curvature of the worldsheet, the six Lovelock conditions, and the Einstein field equations[M/OL]. Zenodo, 2026. https://doi.org/10.5281/zenodo.23395358 [in Chinese]
11. Xu S. ExB-T rotating standing-wave soliton theory: framework, logic chain, and literature review[M/OL]. Zenodo, 2026. https://doi.org/10.5281/zenodo.23452890 [in Chinese]
12. Xu S. Density dependence of the gravitational constant: the ExB-T prediction $G \propto \rho^{-1/2}$ and its compatibility test with SPARC rotation curves[M/OL]. Zenodo, 2026. https://doi.org/10.5281/zenodo.23799439 [in Chinese]
13. Xu S. Stability and mode transitions of rotating standing-wave solitons: a structural isomorphism argument within the wave-ontology framework[M/OL]. Zenodo, 2026. https://doi.org/10.5281/zenodo.23916497 [in Chinese]
14. Gell-Mann M, Low F E. Quantum electrodynamics at small distances[J]. Physical Review, 1954, 95: 1300–1312. https://doi.org/10.1103/PhysRev.95.1300
15. Rosner J L. Higher-order contributions to the divergent part of Z_3 in a model quantum electrodynamics[J]. Annals of Physics, 1967, 44: 11–34. https://doi.org/10.1016/0003-4916(67)90262-X
16. Gorishny S G, Kataev A L, Larin S A, Surguladze L R. The analytic four-loop corrections to the QED β-function in the MS scheme and to the QED ψ-function: total reevaluation[J]. Physics Letters B, 1991, 256: 81–86.
17. Kataev A L, Larin S A. Analytical five-loop expressions for the renormalization group QED β-function in different renormalization schemes[J]. JETP Letters, 2012, 96: 61–65. https://doi.org/10.1134/S0021364012130073
18. Baikov P A, Chetyrkin K G, Kühn J H. Vector correlator in massless QCD at order $O(\alpha_s^4)$ and the QED β-function at five loop[J]. arXiv:1206.1284 [hep-ph], 2012. https://arxiv.org/abs/1206.1284
19. Yuan J, Li G H. Underwater target recognition with sonar fingerprint[C]//Advances in Machine Learning and Cybernetics, LNCS 3930. Springer, 2006: 984–993. https://doi.org/10.1007/11739685_103
20. Hashmi M A R, Raza R H. Landmark based audio fingerprinting for naval vessels[C]//2016 International Conference on Frontiers of Information Technology (FIT). IEEE, 2017: 297–302. https://doi.org/10.1109/FIT.2016.061
21. Salvador S, Chan P. FastDTW: Toward accurate dynamic time warping in linear time and space[J]. Intelligent Data Analysis, 2007, 11: 561–580.
22. Ramsay J O, Silverman B W. Functional Data Analysis[M]. 2nd ed. New York: Springer, 2005.
23. Haverkamp B E. Confirmatory bias in hypothesis testing for client-identified and counselor self-generated hypotheses[J]. Journal of Counseling Psychology, 1993, 40: 303–315. https://doi.org/10.1037/0022-0167.40.3.303
24. Heesen R. Why the reward structure of science makes reproducibility problems inevitable[J]. Journal of Philosophy, 2018.
25. Rubin M. The replication crisis is less of a "crisis" in Lakatos' philosophy of science than it is in Popper's[J]. European Journal for Philosophy of Science, 2025, 15.
26. Fanelli D. Do pressures to publish increase scientists' bias? An empirical support from US states data[J]. PLoS One, 2010, 5: e10271. https://doi.org/10.1371/journal.pone.0010271
27. Filonov N, Levitin M, Polterovich I, Sher D. Uniform enclosures for the phase and zeros of Bessel functions and their derivatives[J]. SIAM Journal on Mathematical Analysis, 2024, 56: 7644–7682.
28. Jiang T. A note on zeros of derivatives of ultraspherical Bessel functions[J]. Journal of Mathematical Analysis and Applications, 2026, 559: 130483. https://doi.org/10.1016/j.jmaa.2026.130483
29. Leuchs G, Sánchez-Soto L L. Light and divergences: History and outlook[J]. arXiv:2507.19569 [physics.hist-ph], 2025. https://arxiv.org/abs/2507.19569
30. Srivastava A, Klassen E P. Functional and Shape Data Analysis[M]. New York: Springer, 2016.
31. Mishra S, Tiwari A. Exploring approaches for curve similarity: A comprehensive review[J]. International Journal of Mathematical Sciences and Computing, 2026, 12.

Supplementary Files

This is a list of supplementary files associated with this preprint. Click to download.

- ExBT.xlsx